INTERNATIONAL JOURNAL FOR NUMERICAL METHODS IN FLUIDS, VOL. 5, 873–890 (1985)

A TRANSIENT SOLUTION METHOD FOR THE FINITE ELEMENT INCOMPRESSIBLE NAVIER–STOKES EQUATIONS

YUTAKA YOSHIDA* AND TAKASHI NOMURA†

Department of Civil Engineering, Tokyo Institute of Technology, 12-1, O-okayama 2 chome, Meguro-ku, Tokyo 152, Japan

SUMMARY

A numerical procedure for solving the time-dependent, incompressible Navier–Stokes equations is presented. The present method is based on a set of finite element equations of the primitive variable formulation, and a direct time integration method which has unique features in its formulation as well as in its evaluation of the contribution of external functions. Particular processes regarding the continuity conditions and the boundary conditions lead to a set of non-linear recurrence equations which represent evolution of the velocities and the pressures under the incompressibility constraint. An iteration process as to the non-linear convective terms is performed until the convergence is achieved in every integration step. Excessively artificial techniques are not introduced into the present solution procedure. Numerical examples with vortex shedding behind a rectangular cylinder are presented to illustrate the features of the proposed method. The calculated results are compared with experimental data and visualized flow fields in literature.

KEY WORDS Incompressible Navier–Stokes Equations Finite Element Method Direct Time Integration Method Vortex Shedding Behind an Obstacle

INTRODUCTION

The Navier–Stokes equations for viscous incompressible fluids possess difficulties in solving them due to the non-linear convective terms as well as the incompressibility constraint imposed by the continuity equation. Since exact solutions of these equations are restricted to idealized cases, numerous researches have been devoted to the development of efficient and accurate numerical methods. The finite element method has received remarkable attention in this field because of a considerable potential for versatile solution procedures.[1,2] Such potential originates in its ease in handling very complex geometries and the ability to naturally incorporate differential-type boundary conditions. Among available combinations of the solution variables, the methods using primitive variables are considered important primarily because these variables are more physical, have lower order equations, and this form of equations provides a relatively straightforward extension to three dimensions. However, the difficulties involved in the basic equations are still retained in the primitive variable approaches.

Important achievements regarding the development of solution procedures have been focused on the following issues: (i) acceptable spatial discretization in mixed interpolations,[3–10] (ii) proper treatments for handling the incompressibility constraint,[11–15] (iii) efficient methods for the convection operators[16–20] and (iv) accurate and efficient time integration algorithms.[21–23] On

* Professor
† Research Associate

0271–2091/85/100873–18$01.80

Received 6 October 1983
Revised 8 April 1985

each of these issues, a number of numerical techniques have been proposed in the literature (among which only typical researches are mentioned above), where various controversial viewpoints still remain inconclusively. Such a situation must be due to the complexity of the objective problems where an adopted numerical technique in addressing one of those issues may restrict or affect the characteristics of the techniques employed for the other issues. For instance, the properties of the time integration scheme cause considerable effects on the algorithm to impose the incompressibility constraint, or on the treatment of the non-linear terms. In this case, the accuracy, the stability, or the computational efficiency of a solution procedure are rather dependent upon synthesized characteristics of the solution algorithm.

The present paper is devoted to describe a solution procedure of the time-dependent, incompressible finite element Navier–Stokes equations of the primitive variable formulation.

A direct time integration method developed by the authors[29,30] is applied to the integration of the finite element equations which are derived via the conventional Galerkin finite element method. The integration method has unique features in its formulation as well as in its evaluation of the contribution of external functions. An attempt to impose the continuity conditions leads to a set of non-linear recurrence equations which represent evolution of the velocities and the pressures under the incompressibility constraint. As for the non-linear terms, an iterative process is performed until the convergence is achieved in every integration step.

Excessively artificial techniques are not introduced throughout the constitution of the present solution procedure. As a consequence, relatively complicated computational processes may be needed to implement the present solution procedure. However, the obtained solution procedure can start only specifying the physical data which can be prescribed from the conditions of the objective problems.

The accuracy of the proposed procedure is verified by comparing the numerical results of flows around a rectangular cylinder with experimental data in the literature.[24–28]

THE FINITE ELEMENT EQUATIONS

The conventional Galerkin finite element spatial discretization of the Navier–Stokes equations and the continuity equation leads to the following systems of coupled ordinary differential equations (cf., for instance Reference 1).

The equations of motion:

$$\mathbf{M}\dot{\mathbf{u}} + \tilde{\mathbf{K}}\mathbf{u} + \mathbf{K}\mathbf{u} + \mathbf{K}_p\mathbf{p} = \mathbf{f}; \quad \dot{\mathbf{u}} \equiv \frac{\mathrm{d}\mathbf{u}}{\mathrm{d}t}. \tag{1}$$

The equations of continuity:

$$\mathbf{K}_p^{\mathrm{T}}\mathbf{u} = \mathbf{0}, \tag{2}$$

where $\mathbf{u}$, $\mathbf{p}$ and $\mathbf{f}$ are the vectors of the nodal velocities, the pressures and the nodal forces, respectively. $\mathbf{M}$, $\tilde{\mathbf{K}} = \tilde{\mathbf{K}}(\mathbf{u})$, $\mathbf{K}$ and $\mathbf{K}_p$ are the coefficient matrices with respect to the density, the convection, the viscosity and the gradient operator. These matrices can be written in terms of the velocity interpolation function $\mathbf{N}_u$ and the pressure interpolation function $\mathbf{N}_p$ as follows:

$$\mathbf{M} = \int\int_\Omega \rho \mathbf{N}_u^{\mathrm{T}}\mathbf{N}_u \mathrm{d}\Omega, \quad \tilde{\mathbf{K}} = \int\int_\Omega \rho \mathbf{N}_u^{\mathrm{T}}\{\nabla(\mathbf{N}_u\mathbf{u})^{\mathrm{T}}\}^{\mathrm{T}}\mathbf{N}_u \mathrm{d}\Omega, \tag{3a, b}$$

$$\mathbf{K} = \int\int_\Omega \mathbf{N}_u^{\mathrm{T}}\mathbf{L}^{\mathrm{T}}\mathbf{D}\mathbf{L}\mathbf{N}_u \mathrm{d}\Omega, \quad \mathbf{K}_p = \int\int_\Omega \mathbf{N}_u^{\mathrm{T}}\mathbf{L}^{\mathrm{T}}\mathbf{m}\mathbf{N}_p \mathrm{d}\Omega, \tag{3c, d}$$

$$\mathbf{f} = \int\int_\Omega \mathbf{N}_u^{\mathrm{T}}\mathbf{b}\mathrm{d}\Omega + \int_{\Gamma_\sigma} \mathbf{N}_u^{\mathrm{T}}\bar{\mathbf{t}}\mathrm{d}\Gamma, \tag{3e}$$

where Ω denotes the objective domain. The boundary of Ω is divided into Γ_u and Γ_σ, where the velocities and the tractions $\mathbf{t}$ are prescribed, respectively. ρ denotes the density and $\mathbf{b}$ the vector of the body forces. The other symbols denote:

$$\nabla = \left\langle \frac{\partial}{\partial x} \quad \frac{\partial}{\partial y} \right\rangle^{\mathrm{T}}, \quad \mathbf{m} = \langle -1 \quad -1 \quad 0 \rangle^{\mathrm{T}}, \tag{4a, b}$$

$$\mathbf{D} = \mu \begin{bmatrix} 2 & 0 & 0 \\ 0 & 2 & 0 \\ 0 & 0 & 1 \end{bmatrix}, \quad \mathbf{L} = \begin{bmatrix} \dfrac{\partial}{\partial x} & 0 & \dfrac{\partial}{\partial y} \\ 0 & \dfrac{\partial}{\partial y} & \dfrac{\partial}{\partial x} \end{bmatrix}^{\mathrm{T}}, \tag{4c, d}$$

in which μ is the coefficient of viscosity.

In equations (1) and (2), the boundary conditions are incorporated in the vectors $\mathbf{u}$ and $\mathbf{f}$ as

$$\mathbf{u} = \langle (\mathbf{u}^\alpha)^{\mathrm{T}} \quad (\bar{\mathbf{u}}^\beta)^{\mathrm{T}} \rangle^{\mathrm{T}}, \tag{5a}$$

$$\mathbf{f} = \langle (\bar{\mathbf{f}}^\alpha)^{\mathrm{T}} \quad (\mathbf{f}^\beta)^{\mathrm{T}} \rangle^{\mathrm{T}}, \tag{5b}$$

where the superposed bar denotes the prescribed components. $\mathbf{f}^\beta$ is the vector of reaction components on Γ_u.

In the present study, the ordinary triangular element with linear interpolation function is used for the velocity field and the pressure is assumed to be constant in each element. If the objective domain can be subdivided into quadrilateral subdomains, a quadrilateral element with one pressure variable, which can be obtained by averaging four triangular elements, will be preferred because of better property with respect to effects of element orientation.

A TIME INTEGRATION METHOD OF FIRST-ORDER INITIAL VALUE PROBLEMS

As the basis of the present solution procedure, a direct time integration method has been developed by the authors[29,30] to solve the initial value problems of the following first-order matrix ordinary differential equations

$$\mathbf{M}\dot{\mathbf{u}} + \mathbf{K}\mathbf{u} = \mathbf{r}, \tag{6}$$

where $\mathbf{r}$ denotes known external functions of the time t, and the coefficient matrix $\mathbf{M}$ is assumed to be symmetric and definite.

The initial conditions for (6) are:

$$\mathbf{u} = \mathbf{u}_0, \quad \text{at } t = 0. \tag{7}$$

The formulation of the integration method is described in the following.

A variational functional corresponding to the initial value problem

By introducing new variables $\boldsymbol{\varphi}$ in terms of which the objective solution variables $\mathbf{u}$ are defined as

$$\mathbf{u} = \mathbf{M}^{-1}(-\mathbf{M}^{\mathrm{T}}\dot{\boldsymbol{\varphi}} + \mathbf{K}^{\mathrm{T}}\boldsymbol{\varphi}), \tag{8}$$

the objective initial value problem of equations (6) and (7) can be transformed into a boundary value problem of the following second-order equations:

$$-\mathbf{M}\ddot{\boldsymbol{\varphi}} + (\mathbf{K}^{\mathrm{T}} - \mathbf{K})\dot{\boldsymbol{\varphi}} + \mathbf{K}\mathbf{M}^{-1}\mathbf{K}^{\mathrm{T}}\boldsymbol{\varphi} = \mathbf{r}, \quad 0 \leqslant t \leqslant T, \tag{9}$$

where T denotes the end of the objective time domain.

The following is an extremum statement equivalent to (9):

$$\pi = \int_0^T [\tfrac{1}{2}(-\mathbf{M}^{\mathrm{T}}\dot{\boldsymbol{\varphi}} + \mathbf{K}^{\mathrm{T}}\boldsymbol{\varphi})^{\mathrm{T}}\mathbf{M}^{-1}(-\mathbf{M}^{\mathrm{T}}\dot{\boldsymbol{\varphi}} + \mathbf{K}^{\mathrm{T}}\boldsymbol{\varphi}) - \boldsymbol{\varphi}^{\mathrm{T}}\mathbf{r}]\mathrm{d}t - [\boldsymbol{\varphi}^{\mathrm{T}}\mathbf{h}]_0^T, \tag{10}$$

in which $\mathbf{h}$ is the vector of natural variables corresponding to $\boldsymbol{\varphi}$.

Under the following essential boundary conditions at $t = T$:

$$\boldsymbol{\varphi}|_{t=T} = \mathbf{0}, \quad \text{at } t = T, \tag{11}$$

the stationary condition of the functional π (10) leads to two sets of the Eulerian equations. One set of them coincides with (9) and the other is the following natural boundary conditions at $t = 0$:

$$-\mathbf{M}\dot{\boldsymbol{\varphi}} + \mathbf{K}^{\mathrm{T}}\boldsymbol{\varphi} + \mathbf{h} = \mathbf{0}, \quad \text{at } t = 0. \tag{12}$$

According to the definition of (8), equation (12) can be rewritten as follows:

$$\mathbf{h} = -\mathbf{M}\mathbf{u} = -\mathbf{M}\mathbf{u}_0. \tag{13}$$

It can be understood that equation (13) corresponds to the initial conditions (7).

Application of the finite element technique

The objective time domain $0 \leqslant t \leqslant T$ is subdivided into a number of subdomains $t_i \leqslant t \leqslant t_{i+1} (= t_i + \Delta t)$, and essential parameters $\boldsymbol{\varphi}_i$ $(= \boldsymbol{\varphi}|_{t=t_i})$ are introduced at the nodal time instant t_i (cf. Figure 1).

When the integral of the functional π (10) is evaluated using the following linear interpolation within a subdomain $t_i \leqslant t \leqslant t_{i+1} (= t_i + \Delta t)$

$$\boldsymbol{\varphi} = \begin{bmatrix} \ulcorner & \urcorner \\ 1 & t \\ \llcorner & \lrcorner \end{bmatrix} \begin{bmatrix} \ulcorner & \urcorner \\ 1 & 0 \\ \llcorner & \lrcorner \\ \ulcorner & \urcorner \\ 1 & \Delta t \\ \llcorner & \lrcorner \end{bmatrix}^{-1} \begin{Bmatrix} \boldsymbol{\varphi}_i \\ \boldsymbol{\varphi}_{i+1} \end{Bmatrix}, \tag{14}$$

where $\ulcorner\ \lrcorner$ denotes a diagonal matrix, the stationary condition of the resulting expression of π leads to the following relationship between essential parameters $\boldsymbol{\varphi}_i$ and natural parameters $\mathbf{h}_i (= -\mathbf{M}\mathbf{u}_i)$ for a typical time interval $t_i \leqslant t \leqslant t_{i+1}$:

$$\begin{bmatrix} \boldsymbol{\Lambda}_{11} & \boldsymbol{\Lambda}_{12} \\ \boldsymbol{\Lambda}_{21} & \boldsymbol{\Lambda}_{22} \end{bmatrix} \begin{Bmatrix} \boldsymbol{\varphi}_i \\ \boldsymbol{\varphi}_{i+1} \end{Bmatrix} = \begin{Bmatrix} \mathbf{M}\mathbf{u}_i \\ -\mathbf{M}\mathbf{u}_{i+1} \end{Bmatrix} + \begin{Bmatrix} \mathbf{r}_{i,i+1} \\ \mathbf{r}_{i+1,i} \end{Bmatrix}, \tag{15}$$

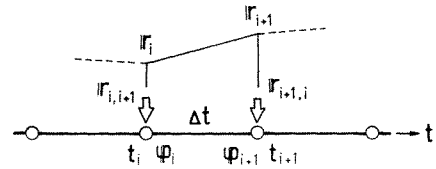

Figure 1. Discretization of the time domain: nodal parameters and equivalent nodal loadings

where the submatrices Λ_{ij} can be given as follows:

$$\Lambda_{11} = \frac{\Delta t}{3}\mathbf{K}\mathbf{M}^{-1}\mathbf{K}^{\mathrm{T}} + \tfrac{1}{2}(\mathbf{K}^{\mathrm{T}} + \mathbf{K}) + \frac{1}{\Delta t}\mathbf{M}, \tag{16a}$$

$$\Lambda_{12} = \frac{\Delta t}{6}\mathbf{K}\mathbf{M}^{-1}\mathbf{K}^{\mathrm{T}} + \tfrac{1}{2}(\mathbf{K}^{\mathrm{T}} - \mathbf{K}) - \frac{1}{\Delta t}\mathbf{M}, \tag{16b}$$

$$\Lambda_{21} = \Lambda_{12}^{\mathrm{T}}, \tag{16c}$$

$$\Lambda_{22} = \frac{\Delta t}{3}\mathbf{K}\mathbf{M}^{-1}\mathbf{K}^{\mathrm{T}} - \tfrac{1}{2}(\mathbf{K}^{\mathrm{T}} + \mathbf{K}) + \frac{1}{\Delta t}\mathbf{M}. \tag{16d}$$

The vectors $\mathbf{r}_{i,i+1}$ and $\mathbf{r}_{i+1,i}$ are the equivalent nodal loadings which result from the weighted integral of the external functions $\mathbf{r}$. Assuming that the functions $\mathbf{r}$ are piecewise linear within an interval $t_i \leqslant t \leqslant t_{i+1}$ as shown in Figure 1, $\mathbf{r}_{i,i+1}$ and $\mathbf{r}_{i+1,i}$ can be given as

$$\mathbf{r}_{i,i+1} = \frac{\Delta t}{6}(2\mathbf{r}_i + \mathbf{r}_{i+1}), \tag{17a}$$

$$\mathbf{r}_{i+1,i} = \frac{\Delta t}{6}(\mathbf{r}_i + 2\mathbf{r}_{i+1}), \tag{17b}$$

where $\mathbf{r}_i = \mathbf{r}|_{t=t_i}$.

A step-by-step time integration formula

When the foregoing single subdomain $t_i \leqslant t \leqslant t_{i+1}$ $(= t_i + \Delta t)$ is regarded as the objective integration time domain $0 \leqslant t \leqslant T$, the essential boundary conditions (11) correspond to the following conditions:

$$\boldsymbol{\varphi}_{i+1} = \mathbf{0}, \quad \text{at } t = t_{i+1}. \tag{18}$$

Imposing (18) on (15) yields a recurrence relationship from t_i to t_{i+1} of the objective variables $\mathbf{u}$ as follows:

$$\Lambda_{11}\boldsymbol{\varphi}_i = \mathbf{M}\mathbf{u}_i + \frac{\Delta t}{3}\mathbf{r}_i + \frac{\Delta t}{6}\mathbf{r}_{i+1}, \tag{19a}$$

$$\mathbf{M}\mathbf{u}_{i+1} = \frac{\Delta t}{6}\mathbf{r}_i + \frac{\Delta t}{3}\mathbf{r}_{i+1} - \Lambda_{21}\boldsymbol{\varphi}_i, \tag{19b}$$

where Δt is now the integration interval.

One step of the time integration consists of the following two processes. First, the variables $\boldsymbol{\varphi}_i$ can be obtained by solving (19a) under the previous values $\mathbf{u}_i$ and the loading terms $\mathbf{r}_i$ and $\mathbf{r}_{i+1}$. Secondly, the objective variables $\mathbf{u}_{i+1}$ can be given by solving (19b) under $\boldsymbol{\varphi}_i$, $\mathbf{r}_i$ and $\mathbf{r}_{i+1}$.

Characteristics of the time integration method

The following single variable system is dealt with as an example to verify the performance of the present integration scheme:

$$\dot{u} + \omega u = c; \quad \omega, c = \text{const.} \tag{20}$$

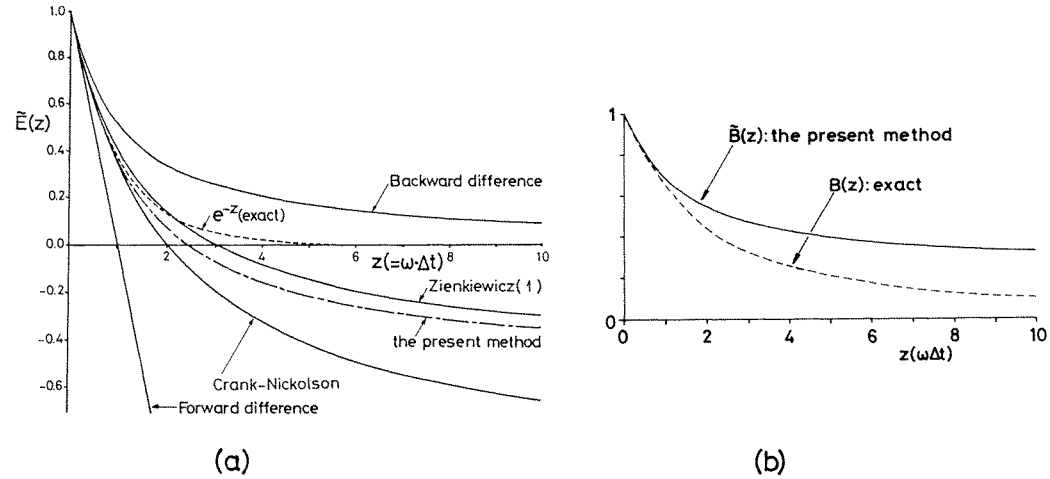

Figure 2. Characteristics of the present direct integration method: (a) characteristic function of the integration operator (compared to some conventional schemes); (b) characteristic of approximated external function

The exact recurrence of (20) can be written as follows:

$$u_{i+1} = E(z)u_i + c\Delta t B(z)$$
$$= \mathrm{e}^{-z}u_i + c\Delta t \frac{1-\mathrm{e}^{-z}}{z}, \tag{21}$$

where $z = \omega\Delta t$.

On the other hand, equation (21) is approximated by means of the present integration method as:

$$u_{i+1} = \tilde{E}(z)u_i + c\Delta t\tilde{B}(z)$$
$$= \frac{-z^2+6}{2z^2+6z+6}u_i + c\Delta t\frac{z^2+6z+12}{4z^2+12z+12}. \tag{22}$$

The functions $\tilde{E}(z)$ and $\tilde{B}(z)$, respectively, indicate the characteristics of the present integration operator, and that of the approximated contribution of the external function. The variation of the approximated functions $\tilde{E}(z)$ and $\tilde{B}(z)$ against $z = \omega\Delta t$ are shown in Figures 2(a) and 2(b) in comparison with the exact functions $E(z)$ and $B(z)$, respectively. The function $\tilde{E}(z)$ approaches the value of $-1/2$ for a large integration interval. The characteristics of conventional single step schemes are also plotted in Figure 2(a) for comparison.[1] A feature of the present time integration formula is that contributions of external functions are evaluated so as to be consistent with the accuracy of the integration operator.

SOLUTION ALGORITHM OF FINITE ELEMENT NAVIER–STOKES EQUATIONS

Application of the time integration formula

Transposing the pressure gradient term $\mathbf{K}_p\mathbf{p}$ and the non-linear term $\tilde{\mathbf{K}}\mathbf{u}$ of the finite element equations of motion (1) to the right-hand side, and treating these terms as external functions, yields

$$\mathbf{M}\dot{\mathbf{u}} + \mathbf{K}\mathbf{u} = \mathbf{f} - \mathbf{K}_p\mathbf{p} - \tilde{\mathbf{K}}\mathbf{u} \equiv \mathbf{r}, \tag{23}$$

where the vectors $\mathbf{u}$ and $\mathbf{f}$, respectively, contain prescribed components and unknown ones as

denoted in (5a, b). The time integration formula (19a, b) is applied to (23) without removing the equations corresponding to the degrees of the nodal reactions $\mathbf{f}^{\beta}$. By this treatment, it is intended to evaluate all components of the nodal accelerations $\dot{\mathbf{u}}$ by means of the present integration operator.

Consequently a set of recurrence equations for a typical time interval from t_i to t_{i+1} are obtained as follows:

$$\mathbf{\Lambda}_{11}\boldsymbol{\varphi}_i = \mathbf{M}\mathbf{u}_i + \frac{\Delta t}{3}\mathbf{r}_i + \frac{\Delta t}{6}(\mathbf{f}_{i+1} - \mathbf{K}_{\mathrm{p}}\mathbf{p}_{i+1} - \tilde{\mathbf{K}}_{i+1}\mathbf{u}_{i+1}), \tag{24a}$$

$$\mathbf{M}\mathbf{u}_{i+1} = \frac{\Delta t}{6}\mathbf{r}_i + \frac{\Delta t}{3}(\mathbf{f}_{i+1} - \mathbf{K}_{\mathrm{p}}\mathbf{p}_{i+1} - \tilde{\mathbf{K}}_{i+1}\mathbf{u}_{i+1}) - \mathbf{\Lambda}_{21}\boldsymbol{\varphi}_i, \tag{24b}$$

where

$$\mathbf{r}_i = \mathbf{f}_i - \mathbf{K}_{\mathrm{p}}\mathbf{p}_i - \tilde{\mathbf{K}}_i\mathbf{u}_i, \quad \text{at } t = t_i, \tag{25a}$$

$$\tilde{\mathbf{K}}_i = \tilde{\mathbf{K}}(\mathbf{u}_i). \tag{25b}$$

On the above recurrence relations (24a, b), the continuity conditions to be satisfied at the advanced time instant $t = t_{i+1}$ are clearly written as follows:

$$\mathbf{K}_{\mathrm{p}}^{\mathrm{T}}\mathbf{u}_{i+1} = \mathbf{0}. \tag{26}$$

Pre-multiplying (24b) by $\mathbf{M}^{-1}$, the velocities $\mathbf{u}_{i+1}$ can be formally expressed as

$$\mathbf{u}_{i+1} = \mathbf{M}^{-1}\left[\frac{\Delta t}{6}\mathbf{r}_i + \frac{\Delta t}{3}(\mathbf{f}_{i+1} - \mathbf{K}_{\mathrm{p}}\mathbf{p}_{i+1} - \tilde{\mathbf{K}}_{i+1}\mathbf{u}_{i+1}) - \mathbf{\Lambda}_{21}\boldsymbol{\varphi}_i\right]. \tag{27}$$

Substitution of (27) into (26) leads to the following equations:

$$\frac{\Delta t}{3}\mathbf{K}_{\mathrm{p}}^{\mathrm{T}}\mathbf{M}^{-1}\mathbf{K}_{\mathrm{p}}\mathbf{p}_{i+1} = \mathbf{K}_{\mathrm{p}}^{\mathrm{T}}\mathbf{M}^{-1}\left[\frac{\Delta t}{6}\mathbf{r}_i + \frac{\Delta t}{3}(\mathbf{f}_{i+1} - \tilde{\mathbf{K}}_{i+1}\mathbf{u}_{i+1}) - \mathbf{\Lambda}_{21}\boldsymbol{\varphi}_i\right] \tag{28}$$

Since equations (24a, b) and (28) are still unsolvable, owing to the particular process that the unknown components $\mathbf{f}^{\beta}$ have been intentionally left in the vector $\mathbf{f}$, the following procedure is considered to solve these equations.

Fundamental recurrence equations

Concerning the notation used in (5a, b), equations (24a, b) and (28) can be partitioned as follows:

$$\begin{bmatrix}\mathbf{\Lambda}_{11}^{\alpha}\\ \mathbf{\Lambda}_{11}^{\beta}\end{bmatrix}\boldsymbol{\varphi}_i = \begin{bmatrix}\mathbf{M}^{\alpha\alpha}\mathbf{M}^{\alpha\beta}\\ \mathbf{M}^{\beta\alpha}\mathbf{M}^{\beta\beta}\end{bmatrix}\begin{Bmatrix}\mathbf{u}_i^{\alpha}\\ \bar{\mathbf{u}}_i^{\beta}\end{Bmatrix} + \frac{\Delta t}{3}\begin{Bmatrix}\mathbf{r}_i^{\alpha}\\ \mathbf{r}_i^{\beta}\end{Bmatrix} + \frac{\Delta t}{6}\left[\begin{Bmatrix}\bar{\mathbf{f}}_{i+1}^{\alpha}\\ \mathbf{f}_{i+1}^{\beta}\end{Bmatrix} - \begin{bmatrix}\mathbf{K}_{\mathrm{p}}^{\alpha}\\ \mathbf{K}_{\mathrm{p}}^{\beta}\end{bmatrix}\mathbf{p}_{i+1} - \begin{bmatrix}\tilde{\mathbf{K}}_{i+1}^{\alpha}\\ \tilde{\mathbf{K}}_{i+1}^{\beta}\end{bmatrix}\mathbf{u}_{i+1}\right], \tag{29a}$$

$$\begin{bmatrix}\mathbf{M}^{\alpha\alpha} & \mathbf{M}^{\alpha\beta}\\ \mathbf{M}^{\beta\alpha} & \mathbf{M}^{\beta\beta}\end{bmatrix}\begin{Bmatrix}\mathbf{u}_{i+1}^{\alpha}\\ \bar{\mathbf{u}}_{i+1}^{\beta}\end{Bmatrix} = \frac{\Delta t}{6}\begin{Bmatrix}\mathbf{r}_i^{\alpha}\\ \mathbf{r}_i^{\beta}\end{Bmatrix} + \frac{\Delta t}{3}\left[\begin{Bmatrix}\bar{\mathbf{f}}_{i+1}^{\alpha}\\ \mathbf{f}_{i+1}^{\beta}\end{Bmatrix} - \begin{bmatrix}\mathbf{K}_{\mathrm{p}}^{\alpha}\\ \mathbf{K}_{\mathrm{p}}^{\beta}\end{bmatrix}\mathbf{p}_{i+1} - \begin{bmatrix}\tilde{\mathbf{K}}_{i+1}^{\alpha}\\ \tilde{\mathbf{K}}_{i+1}^{\beta}\end{bmatrix}\mathbf{u}_{i+1}\right] - \begin{bmatrix}\mathbf{\Lambda}_{21}^{\alpha}\\ \mathbf{\Lambda}_{21}^{\beta}\end{bmatrix}\boldsymbol{\varphi}_i, \tag{29b}$$

$$\begin{aligned}\frac{\Delta t}{3}\begin{bmatrix}\mathbf{K}_{\mathrm{p}}^{\alpha}\\ \mathbf{K}_{\mathrm{p}}^{\beta}\end{bmatrix}^{\mathrm{T}}\begin{bmatrix}\mathbf{M}^{\alpha\alpha} & \mathbf{M}^{\alpha\beta}\\ \mathbf{M}^{\beta\alpha} & \mathbf{M}^{\beta\beta}\end{bmatrix}^{-1}\begin{bmatrix}\mathbf{K}_{\mathrm{p}}^{\alpha}\\ \mathbf{K}_{\mathrm{p}}^{\beta}\end{bmatrix}\mathbf{p}_{i+1} &= \begin{bmatrix}\mathbf{K}_{\mathrm{p}}^{\alpha}\\ \mathbf{K}_{\mathrm{p}}^{\beta}\end{bmatrix}^{\mathrm{T}}\begin{bmatrix}\mathbf{M}^{\alpha\alpha} & \mathbf{M}^{\alpha\beta}\\ \mathbf{M}^{\beta\alpha} & \mathbf{M}^{\beta\beta}\end{bmatrix}^{-1}\begin{bmatrix}\frac{\Delta t}{6}\begin{Bmatrix}\mathbf{r}_i^{\alpha}\\ \mathbf{r}_i^{\beta}\end{Bmatrix}\\ \\ +\frac{\Delta t}{3}\left(\begin{Bmatrix}\bar{\mathbf{f}}_{i+1}^{\alpha}\\ \mathbf{f}_{i+1}^{\beta}\end{Bmatrix} - \begin{bmatrix}\tilde{\mathbf{K}}_{i+1}^{\alpha}\\ \tilde{\mathbf{K}}_{i+1}^{\beta}\end{bmatrix}\mathbf{u}_{i+1}\right) - \begin{bmatrix}\mathbf{\Lambda}_{21}^{\alpha}\\ \mathbf{\Lambda}_{21}^{\beta}\end{bmatrix}\boldsymbol{\varphi}_i\end{bmatrix}.\end{aligned} \tag{29c}$$

Elimination of the nodal reactions $\mathbf{f}_{i+1}^{\beta}$ from equations (29a–c) is a clue to solve these complicated and coupled equations. In equation (29b) the term $\mathbf{f}_{i+1}^{\beta}$ is coupled with the unknown

velocity components $\mathbf{u}_{i+1}^{\alpha}$ through the submatrix $\mathbf{M}^{\beta\alpha}$. Considering separation of these terms, which is necessary for the elimination of $\mathbf{f}_{i+1}^{\beta}$, it is a natural and simple treatment to delete off-diagonal terms of the consistent mass matrix $\mathbf{M}$ by replacing it with a lumped mass matrix:

$$\mathbf{M}_{\mathrm{L}}=\begin{bmatrix}\mathbf{M}_{\mathrm{L}}^{\alpha} & \mathbf{0}\\ \mathbf{0} & \mathbf{M}_{\mathrm{L}}^{\beta}\end{bmatrix}. \tag{30}$$

As a consequence of mass lumping, the term $\mathbf{f}_{i+1}^{\beta}$ can be explicitly expressed as follows:

$$\mathbf{f}_{i+1}^{\beta}=\frac{3}{\Delta t}\left[\mathbf{M}_{\mathrm{L}}^{\beta}\bar{\mathbf{u}}_{i+1}^{\beta}-\frac{\Delta t}{6}\mathbf{r}_{i}^{\beta}+\frac{\Delta t}{3}(\mathbf{K}_{\mathrm{p}}^{\beta}\mathbf{p}_{i+1}+\tilde{\mathbf{K}}_{i+1}^{\beta}\mathbf{u}_{i+1})+\boldsymbol{\Lambda}_{21}^{\beta}\boldsymbol{\varphi}_{i}\right], \tag{31a}$$

and the unknown velocity components $\mathbf{u}_{i+1}^{\alpha}$ are expressed as

$$\mathbf{u}_{i+1}^{\alpha}=(\mathbf{M}_{\mathrm{L}}^{\alpha})^{-1}\left[\frac{\Delta t}{3}\bar{\mathbf{f}}_{i+1}^{\alpha}+\frac{\Delta t}{6}\mathbf{r}_{i}^{\alpha}-\frac{\Delta t}{3}(\mathbf{K}_{\mathrm{p}}^{\alpha}\mathbf{p}_{i+1}+\tilde{\mathbf{K}}_{i+1}^{\alpha}\mathbf{u}_{i+1})-\boldsymbol{\Lambda}_{21}^{\alpha}\boldsymbol{\varphi}_{i}\right]. \tag{31b}$$

Substituting (31a) into (29a) and (29c) to eliminate $\mathbf{f}_{i+1}^{\beta}$, the following equations are derived:

$$\begin{bmatrix}\boldsymbol{\Lambda}_{11}^{\alpha}\\ \boldsymbol{\Lambda}_{11}^{\beta}-\frac{1}{2}\boldsymbol{\Lambda}_{21}^{\beta}\end{bmatrix}\boldsymbol{\varphi}_{i}=\begin{Bmatrix}\frac{\Delta t}{3}\mathbf{r}_{i}^{\alpha}\\ \frac{\Delta t}{4}\mathbf{r}_{i}^{\beta}\end{Bmatrix}+\frac{\Delta t}{6}\begin{Bmatrix}\bar{\mathbf{f}}_{i+1}^{\alpha}\\ \mathbf{0}^{\beta}\end{Bmatrix}+\frac{\Delta t}{6}\begin{bmatrix}\mathbf{K}_{\mathrm{p}}^{\alpha}\\ \mathbf{0}^{\beta}\end{bmatrix}\mathbf{p}_{i+1}$$
$$-\frac{\Delta t}{6}\begin{bmatrix}\tilde{\mathbf{K}}_{i+1}^{\alpha}\\ \mathbf{0}^{\beta}\end{bmatrix}\mathbf{u}_{i+1}+\begin{Bmatrix}\mathbf{M}_{\mathrm{L}}^{\alpha}\mathbf{u}_{i}^{\alpha}\\ \mathbf{M}_{\mathrm{L}}^{\beta}(\bar{\mathbf{u}}_{i}^{\beta}+\frac{1}{2}\bar{\mathbf{u}}_{i+1}^{\beta})\end{Bmatrix}, \tag{32a}$$

$$\frac{\Delta t}{3}(\mathbf{K}_{\mathrm{p}}^{\alpha})^{\mathrm{T}}(\mathbf{M}_{\mathrm{L}}^{\alpha})^{-1}\mathbf{K}_{\mathrm{p}}^{\alpha}\mathbf{p}_{i+1}=(\mathbf{K}_{\mathrm{p}}^{\alpha})^{\mathrm{T}}(\mathbf{M}_{\mathrm{L}}^{\alpha})^{-1}\left[\frac{\Delta t}{6}\mathbf{r}_{i}^{\alpha}+\frac{\Delta t}{3}(\bar{\mathbf{f}}_{i+1}^{\alpha}-\tilde{\mathbf{K}}_{i+1}^{\alpha}\mathbf{u}_{i+1})-\boldsymbol{\Lambda}_{21}^{\alpha}\boldsymbol{\varphi}_{i}\right]+(\mathbf{K}_{\mathrm{p}}^{\beta})^{\mathrm{T}}\bar{\mathbf{u}}_{i+1}^{\beta}. \tag{32b}$$

Each of equations (32a) and (32b) includes $\boldsymbol{\varphi}_{i}$ and $\mathbf{p}_{i+1}$ as unknowns. Transposing $\boldsymbol{\varphi}_{i}$ and $\mathbf{p}_{i+1}$ of the right-hand side to the left-hand side and rearranging, yields

$$\left[\begin{array}{c|c}\boldsymbol{\Lambda}_{11}^{\alpha} & \frac{\Delta t}{6}\mathbf{K}_{\mathrm{p}}^{\alpha}\\ \boldsymbol{\Lambda}_{11}^{\beta}-\frac{1}{2}\boldsymbol{\Lambda}_{21}^{\beta} & \mathbf{0}^{\beta}\\ \hline (\mathbf{K}_{\mathrm{p}}^{\alpha})^{\mathrm{T}}(\mathbf{M}_{\mathrm{L}}^{\alpha})^{-1}\boldsymbol{\Lambda}_{21}^{\alpha} & \frac{\Delta t}{3}(\mathbf{K}_{\mathrm{p}}^{\alpha})^{\mathrm{T}}(\mathbf{M}_{\mathrm{L}}^{\alpha})^{-1}\mathbf{K}_{\mathrm{p}}^{\alpha}\end{array}\right]\begin{Bmatrix}\boldsymbol{\varphi}_{i}\\ \hline \mathbf{p}_{i+1}\end{Bmatrix}$$
$$=\left\{\begin{array}{l}\begin{Bmatrix}\frac{\Delta t}{3}\mathbf{r}_{i}^{\alpha}\\ \frac{\Delta t}{4}\mathbf{r}_{i}^{\beta}\end{Bmatrix}+\frac{\Delta t}{6}\begin{Bmatrix}\bar{\mathbf{f}}_{i+1}^{\alpha}\\ \mathbf{0}^{\beta}\end{Bmatrix}-\frac{\Delta t}{6}\begin{bmatrix}\tilde{\mathbf{K}}_{i+1}^{\alpha}\\ \mathbf{0}^{\beta}\end{bmatrix}\mathbf{u}_{i+1}+\begin{Bmatrix}\mathbf{M}_{\mathrm{L}}^{\alpha}\mathbf{u}_{i}^{\alpha}\\ \mathbf{M}_{\mathrm{L}}^{\beta}(\bar{\mathbf{u}}_{i}^{\beta}+\frac{1}{2}\bar{\mathbf{u}}_{i+1}^{\beta})\end{Bmatrix}\\ \hline (\mathbf{K}_{\mathrm{p}}^{\alpha})^{\mathrm{T}}(\mathbf{M}_{\mathrm{L}}^{\alpha})^{-1}\left[\frac{\Delta t}{6}\mathbf{r}_{i}^{\alpha}+\frac{\Delta t}{3}(\bar{\mathbf{f}}_{i+1}^{\alpha}-\tilde{\mathbf{K}}_{i+1}^{\alpha}\mathbf{u}_{i+1})\right]+(\mathbf{K}_{\mathrm{p}}^{\beta})^{\mathrm{T}}\bar{\mathbf{u}}_{i+1}^{\beta}\end{array}\right\} \tag{33}$$

Equations (31a, b) and (33) are the fundamental recurrence equations of the proposed solution procedure.

Solution algorithm

Regarding the non-linear term $\tilde{\mathbf{K}}_{i+1}\mathbf{u}_{i+1}$, the following simple iterative procedure is performed during one integration step from t_i to t_{i+1}.

(i) The right-hand side of (33) is a vector consisting of the known terms at $t = t_i$, the prescribed values at $t = t_{i+1}$ and the non-linear term $\tilde{\mathbf{K}}_{i+1}\mathbf{u}_{i+1}$ at t_{i+1}. At first $\tilde{\mathbf{K}}_{i+1}\mathbf{u}_{i+1}$ is approximated in terms of the values at $t = t_i$, namely $\tilde{\mathbf{K}}_i\mathbf{u}_i$.
(ii) Then equation (33) can be solved and the first approximations $\boldsymbol{\varphi}_i^{(1)}$ and $\mathbf{p}_{i+1}^{(1)}$ are obtained.
(iii) The non-linear term $\tilde{\mathbf{K}}_{i+1}\mathbf{u}_{i+1}$ of (31a, b) is approximated in terms of the same values that have been used in the process (ii). Substituting $\boldsymbol{\varphi}_i^{(1)}$ and $\mathbf{p}_{i+1}^{(1)}$ into (31a, b), the first approximations of the velocities $\mathbf{u}_{i+1}^{\alpha(1)}$ and the nodal reactions $\mathbf{f}_{i+1}^{\beta(1)}$ can be obtained.
(iv) The non-linear terms are updated to $\tilde{\mathbf{K}}_{i+1}^{(1)}\mathbf{u}_{i+1}^{(1)}$.

The processes (ii) to (iv) are repeated until the following convergence criteria are satisfied:

$$\sqrt{\left(\frac{\|\mathbf{u}_{i+1}^{\alpha(n+1)} - \mathbf{u}_{i+1}^{\alpha(n)}\|}{\|\mathbf{u}_{i+1}^{\alpha(n+1)}\|}\right)} < \varepsilon_{\mathrm{u}}, \quad \sqrt{\left(\frac{\|\mathbf{f}_{i+1}^{\beta(n+1)} - \mathbf{f}_{i+1}^{\beta(n)}\|}{\|\mathbf{f}_{i+1}^{\beta(n+1)}\|}\right)} < \varepsilon_{\mathrm{f}}, \tag{34a, b}$$

$$\sqrt{\left(\frac{\|\mathbf{p}_{i+1}^{(n+1)} - \mathbf{p}_{i+1}^{(n)}\|}{\|\mathbf{p}_{i+1}^{(n+1)}\|}\right)} < \varepsilon_{\mathrm{p}}, \tag{34c}$$

where ε_{u}, ε_{f} and ε_{p} are preassigned error tolerances.

On every updated set of velocities, $\mathbf{u}_{i+1}^{(n)}$, the incompressible continuity conditions (26) have been imposed. The system matrix on the left-hand side of (33) is non-symmetric, and rather complicated processes are required to assemble this matrix. However, the system matrix may possess a band-profile upon appropriate arrangement of the order of the variables in the array $\langle \boldsymbol{\varphi}_i^{\mathrm{T}} \ \mathbf{p}_{i+1}^{\mathrm{T}} \rangle$, to which, for example, so-called skyline storage is adoptable. In addition, as far as the integration interval Δt is fixed, only one factorization need be performed. After that, only the forward-reduction/back-substitution of the factorized array need be repeated in the present solution algorithm.

NUMERICAL EXAMPLES

In this section a series of numerical results for flows past a rectangular cylinder of various width-to-height ratio B/H (B is a side length of a cylinder and H is the height) at different Reynolds numbers (Re) are presented in order to verify the features of the proposed procedure. The calculated flow fields are compared with experimentally observed ones, which are reported in the literature.[24–26] Three cases of computations were performed: (A) $Re = 126$ of $B/H = 0$ (i.e. flat plate), (B) $Re = 150$ of $B/H = 1$ and (C) $Re = 300$ of $B/H = 2$. The finite element mesh and the boundary conditions of Case (B) are shown in Figure 3(a). At the inlet boundary, uniform velocity distribution U is assumed. The outlet boundary is assumed to be traction free. Along the other two boundaries, tangential tractions and the normal velocity components are assumed to be zero. The non-slip condition is prescribed at the cylinder surfaces. Only the side length B was changed for the other two cases.

Case (A): evolution of twin vortices behind a flat plate

In Case (A) it is intended to compare the calculated results with the experimental observations by Taneda and Honji.[24] Their experiment was carried out in a water tank 40 cm wide. A thin

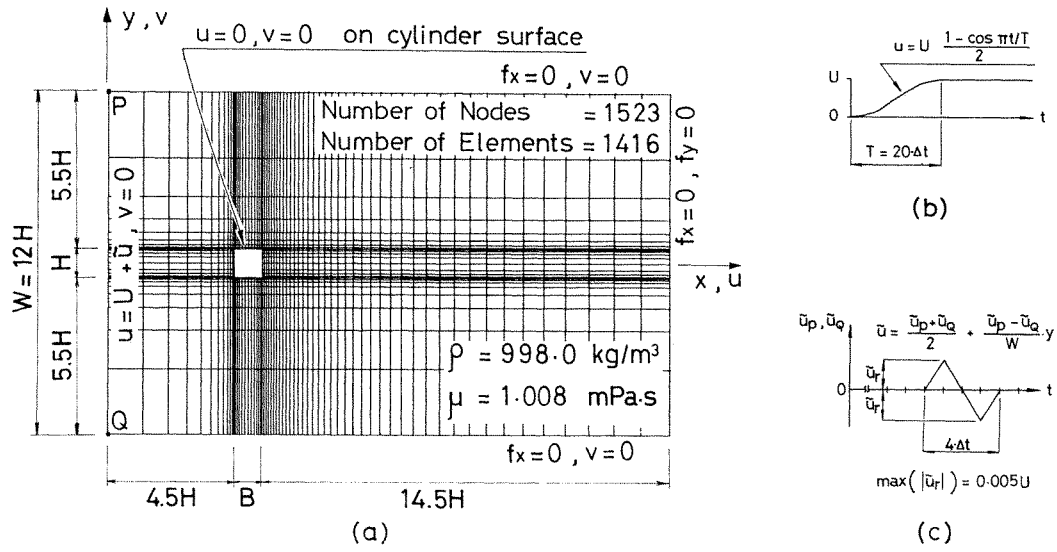

Figure 3. Flow past a rectangular cylinder: (a) finite element mesh and boundary conditions; (b) initial path of the inlet velocity from 0 to U; (c) small perturbation randomly added to the inlet velocity

test plate ($H = 3$ cm) immersed in the water was started from rest impulsively at the velocity $U = 0{\cdot}495$ cm/s (the corresponding Reynolds number is 126). The situation examined in the experiment was interpreted to the foregoing finite element model ($B/H = 0$). The initial conditions were as follows:

$$\mathbf{u} = \mathbf{0}, \quad \mathbf{f} = \mathbf{0} \quad \text{and} \quad \mathbf{p} = 0, \quad \text{at } t = 0. \tag{35}$$

As the inlet velocities were also zero at $t = 0$, these were increased from zero to U along the curve of Figure 3(b) during the initial 20 steps. All the tolerances ε_u, ε_f and ε_p of the convergence criteria (34a–c), were 10^{-3}. The integration interval Δt was 0·5 s (the dimensionless value is 0·0825).

Since the mesh division and the boundary condition were symmetric, the following linear velocity distribution of fairly small amplitude was randomly added to the inlet velocity U as an attempt to perturb the symmetry:

$$\tilde{u} = \tfrac{1}{2}\{\tilde{u}_P(t) + \tilde{u}_Q(t)\} + \{\tilde{u}_P(t) - \tilde{u}_Q(t)\}\left(\frac{y}{W}\right) \tag{36}$$

where W denotes the length of inlet boundary (cf. Figure 3(a)). u_P and u_Q are the velocities at the corners P and Q, respectively. These are functions of the time t, as shown in Figure 3(c), and the magnitude of their peaks was made to be scattered randomly within $\pm 0{\cdot}005U$.

The calculated time history of the stagnation point is compared with the experimental results[24] in Figure 4(a), where the origin of the time of the calculation, t, is appropriately shifted from that of the time of the experiment, t^e, in order to adjust the initial time gap due to the initial treatment in the calculation (cf. Figure 3(b)). Distribution of the instantaneous streamlines observed in the experiment by means of the aluminium dust method is shown in Figure 4(b), which is reproduced by the authors from the photograph in Reference 24. Figures 4(c) and 4(d), respectively, show the calculated velocity and pressure field at the time instant nearest to the actual instant of the experimental observation (Figure 4(b)). These time instants are indicated in Figure 4(a).

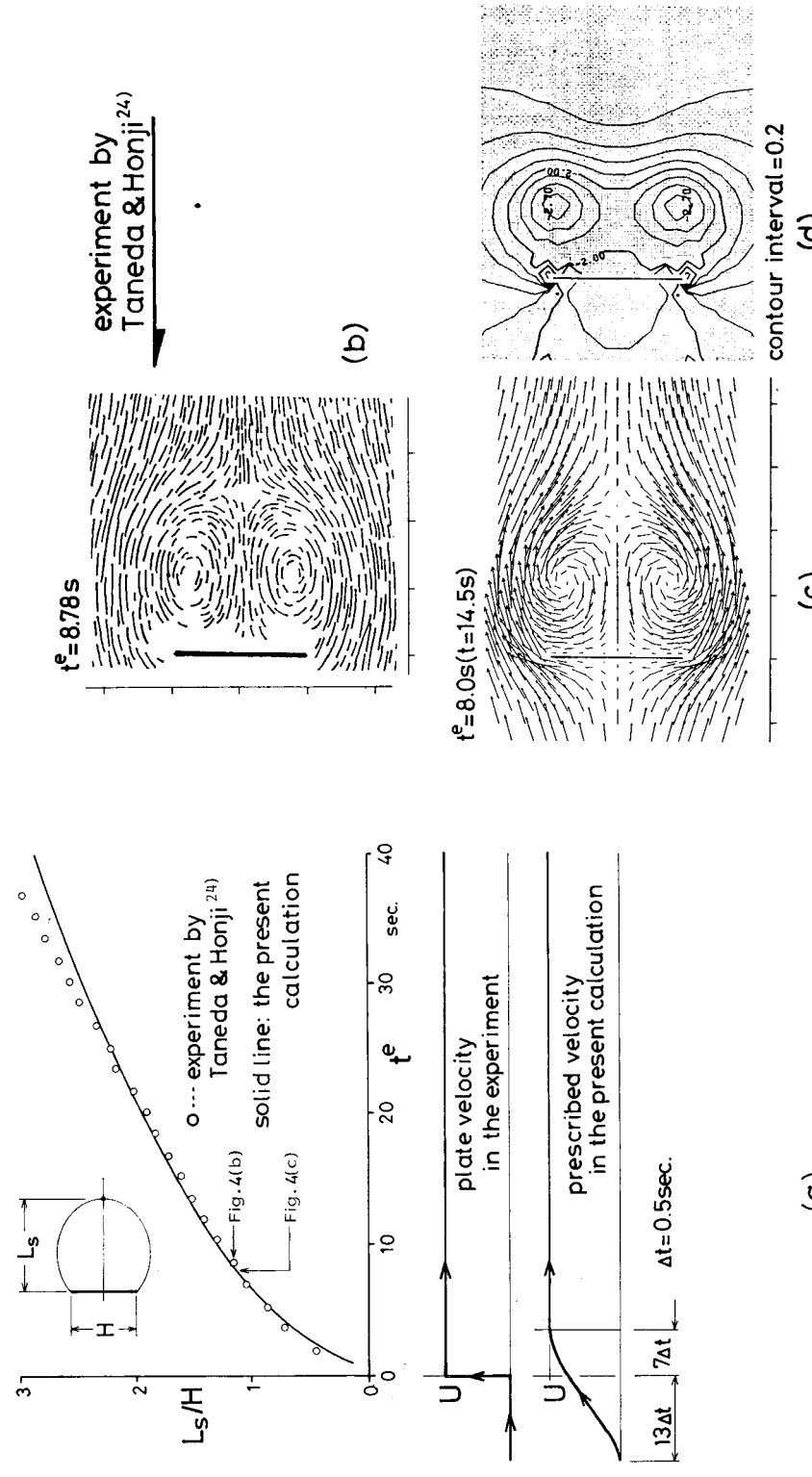

Figure 4. Development of twin vortices behind the flat plate at $Re = 126$: (a) evolutional movement of the stagnation point (comparison with the experimental results of Taneda and Honji[24]); (b) typical instantaneous streamlines visualized by Taneda and Honji[24]—reproduced by the authors from the photograph in Reference 24; (c) calculated velocity vectors; (d) calculated dimensionless pressure contours

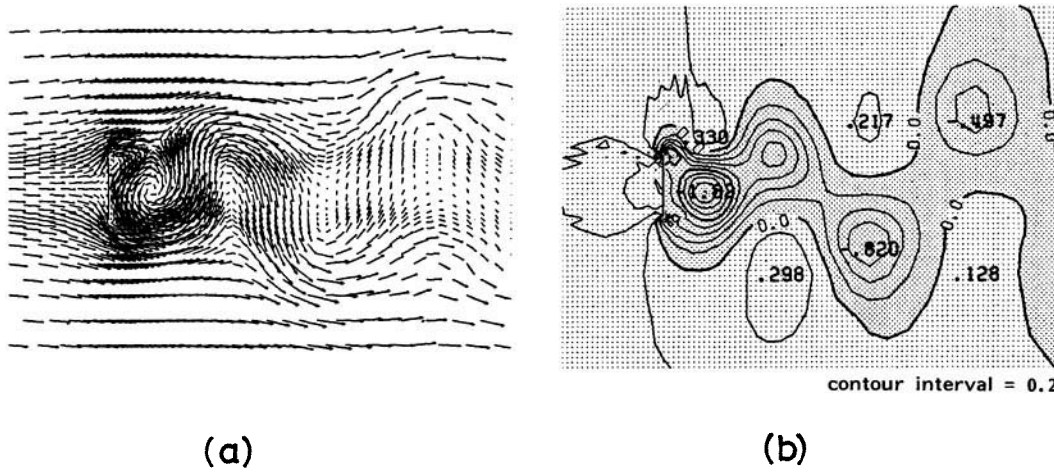

Figure 5. Typical flow field during a regularly periodic shedding: (a) velocity vectors; (b) dimensionless pressure contours

After the flow became asymmetric at about $t = 600$s, the regular periodic shedding began at about $t = 1000$s. As the perturbation was considerably small, the symmetry of the calculated flow continued for fairly long time. Figures 5(a) and 5(b) show the velocity and the pressure distributions at an instant during a typical periodic shedding cycle. The Strouhal number (St) was 0·173. A reported experimental value is about 0·165.[27] Through the present computation the velocity divergence between the inlet boundary and the outlet one was only $O(U \times 10^{-12})$ (the computation was executed in double precision). This indicates that the continuity conditions are accurately satisfied in the present solution procedure. After the regularly periodic vortex shedding was obtained, convergence criteria (34a–c) were satisfied after four iterations per integration step.

Case (B) and (C): flow past a rectangular cylinder

Cases (B) and (C) are devoted to comparison with a series of experiments carried out by Okajima and Sugitani.[25,26] The initial conditions and the initial treatment of the inlet velocity of both cases were the same as Case (A). The integration interval was $\Delta t^* = 0{\cdot}1$, where $t^*(= tU/H)$ denotes the dimensionless time.

Case (B). After the flow became asymmetric at about $t^* = 45$, a regular periodic shedding was attained at about $t^* = 100$. Four iterations per step were needed at this stage. In Figure 6 the calculated velocity distribution is compared with the instantaneous streamlines observed by Okajima[25] (reproduced from his photograph by the authors). It can be seen that the vector directions correspond to the experimental stream directions even at fairly far positions from the cylinder. The evaluated Strouhal number was 0·164, whereas the values reported in the experiment were within 0·14–0·145.[25]

The velocity vectors and the pressure contours during a half cycle of shedding are shown in Figures 7(a)–(c). In Figures 7(d) and 7(e) variations of the drag coefficient C_D, the lift coefficient C_L and non-dimensional pressures $p^*(= p/\rho U^2)$ at each centre of cylinder sides are plotted during a typical cycle of periodic shedding. The drag and lift resulted from direct summation of the nodal reaction components ($\mathbf{f}^B$) on the cylinder surfaces. Therefore, not only the pressure

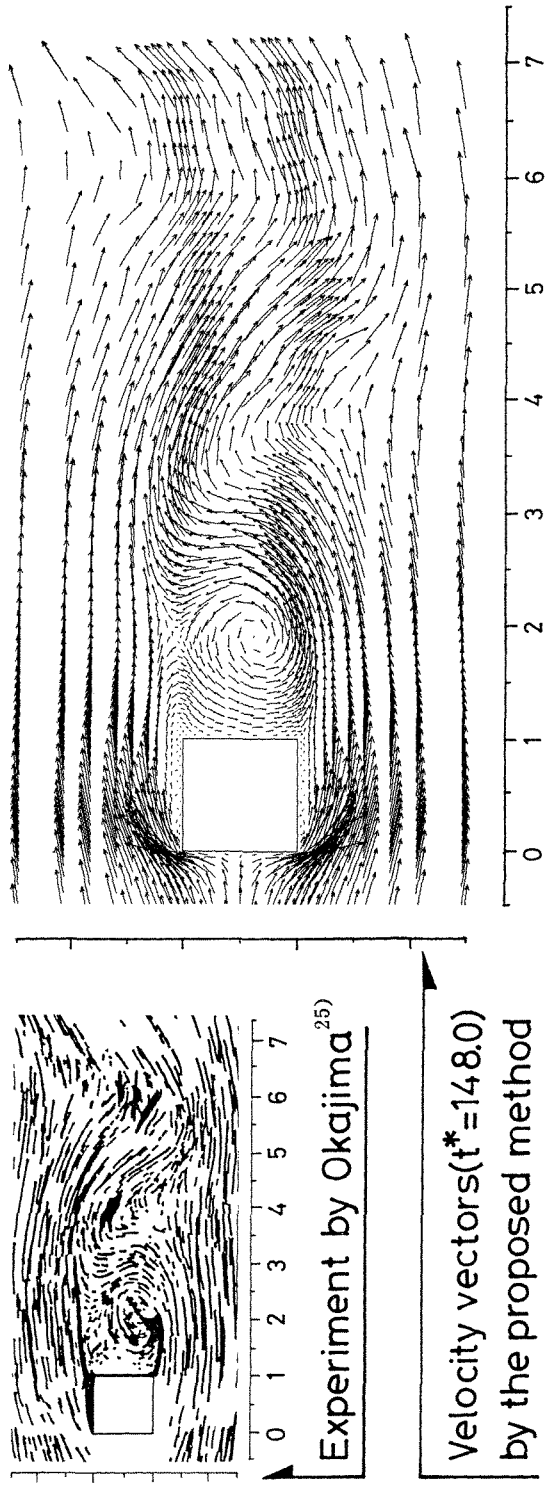

Figure 6. Comparison of the calculated velocity field near the square cylinder at $Re = 150$ with visualized instantaneous streamlines by Okajima[25] (the left figure is reproduced by the authors from the photograph in Reference 25)

but the viscous stresses contribute to these forces. At the peaks of C_L (Figures 7(a) and 7(c)) the flows separated at the leading edges and rolled up behind the cylinder. When C_L was zero (Figure 7(b)), a vortex was going to leave the cylinder. The mean value of C_D was 1·66 and the peak value of C_L was 0·43. A reported experimental value of C_D is about 1·5.[28] The difference of p^* between the side S_2 and S_4 correlated with the variation of C_L, whereas variation of p^* on the

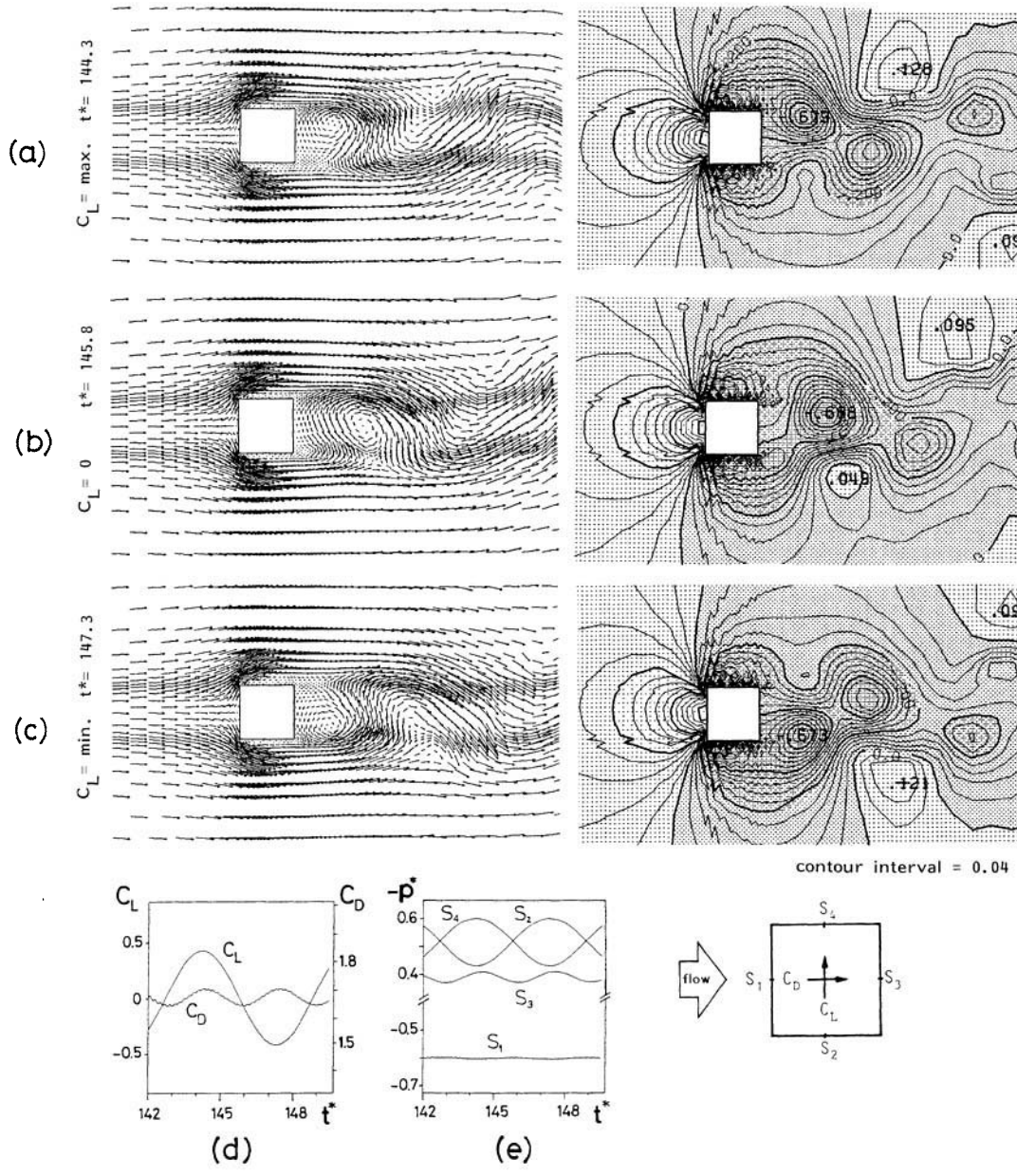

Figure 7. Velocity vectors and dimensionless pressure contours near the square cylinder during regularly periodic sheddings at $Re = 150$: (a) at C_L = max.; (b) at $C_L = 0$; (c) at C_L = min.; (d) time histories of the drag and the lift; (e) time history of the surface pressures

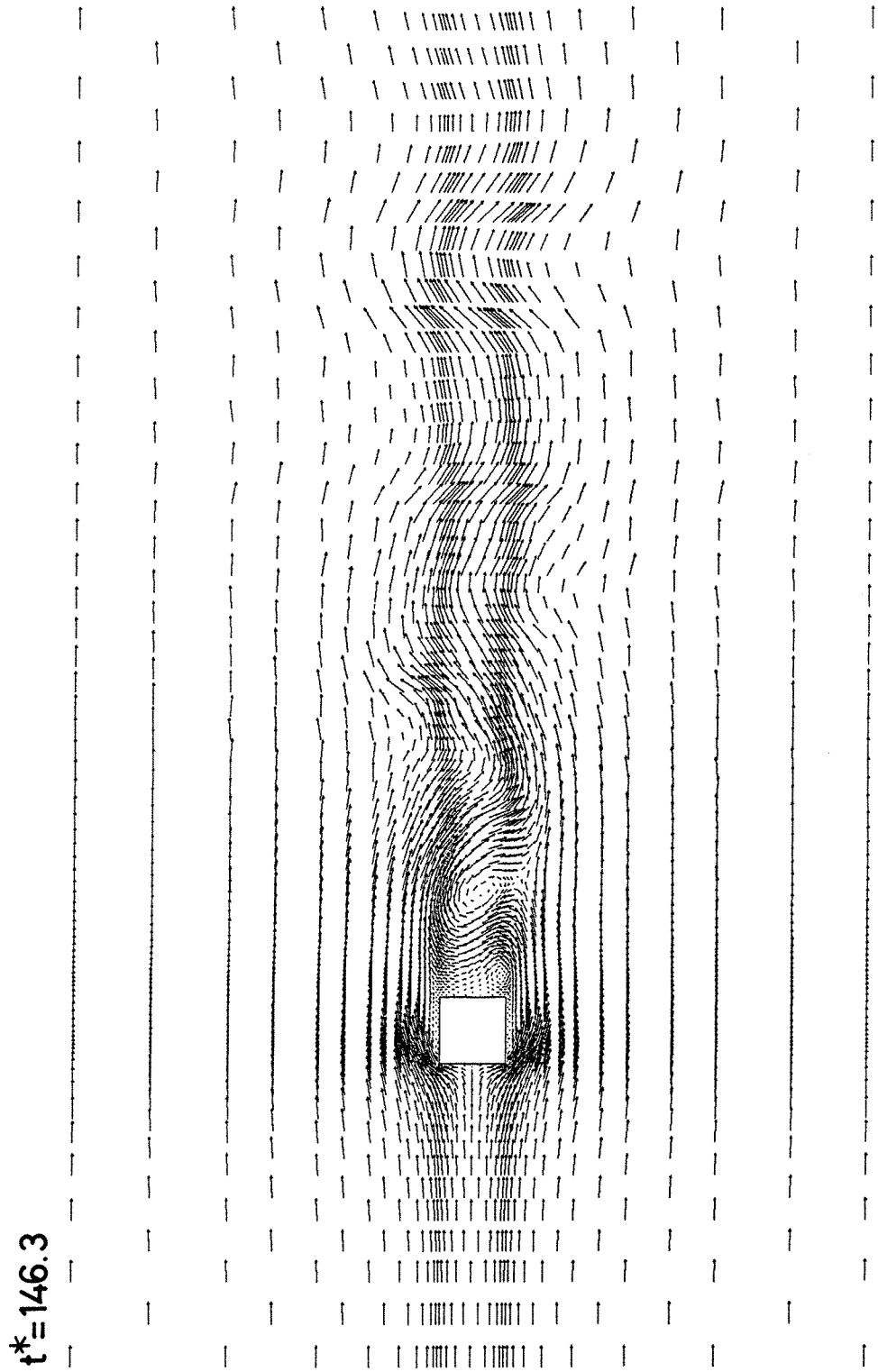

Figure 8. Typical velocity vectors in overall domain ($Re = 150$ and $B/H = 1$)

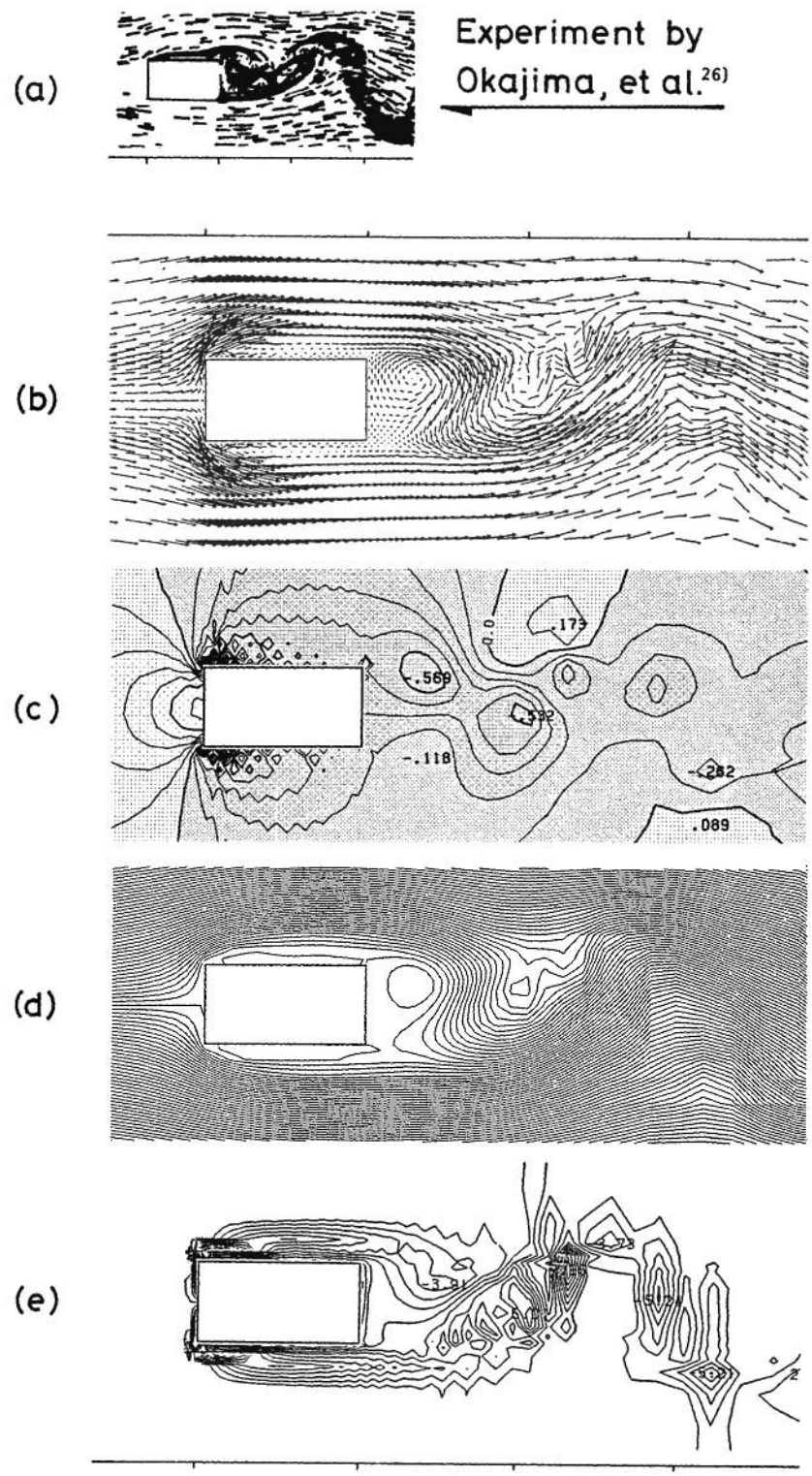

Figure 9. Typical flow fields at $Re = 300$ of $B/H = 2$: (a) instantaneous streamlines and streaklines visualized by Okajima and Sugitani[26] (reproduced from their photograph by the authors); (b) velocity vectors; (c) dimensionless pressure contours; (d) instantaneous streamlines; (e) vorticity contours

back side S_3 correlated with that of C_D. Figure 8 shows typical velocity distribution in overall domain, where the sinusoidally oscillating wake is travelling toward the outlet boundary.

Case (C). At $Re = 300$ the regularity of the oscillation of the wake was slightly fluctuated and the calculated peak value of the Strouhal number was 0·170, whereas the experimental value was somewhat scattered between 0·15 and 0·17.[26] Figure 9(a) is a typical flow field at $Re = 300$ visualized by Okajima and Sugitani[26] (reproduced from their photograph by the authors), who used the aluminium dust method to indicate instantaneous streamlines and the electrolytic precipitation method to indicate streaklines. Figures 9(b)–9(e) show corresponding calculated velocity vectors, pressure contours, instantaneous streamlines and vorticity contours.

CONCLUDING REMARKS

A numerical procedure for unsteady flow problems of viscous incompressible fluids has been presented. The proposed solution procedure is outlined as follows. (i) The spatial discretization of the Navier–Stokes equations and the continuity equation is performed via the finite element method. The ordinary triangular element of linear interpolation is used for the velocity field. The pressure is assumed constant in each element. (ii) A unique direct time integration method is adopted. (iii) The integration formula is applied to the equations of motion without removing the equations corresponding to the degrees of the prescribed velocity components. (iv) After the continuity conditions are imposed on the velocities of the recurrence equations of motion, the boundary conditions are applied and the nodal reaction components are eliminated. (v) An iterative process concerning the non-linear terms is performed at every integration step. Excessively artificial techniques are not introduced into the present solution procedure.

The numerical examples compared to several experimental observations and measurements, have shown that (i) the solutions satisfy the incompressibility conditions; (ii) the time-dependent solutions agree fairly well with the experimentally visualized flow fields reported in the literature; (iii) the fluid forces acting on the obstacles can be predicted in the present calculations.

The capabilities of the proposed solution procedure depend fairly, but not completely, upon the characteristics of the time integration method employed. However, the accuracy of the solutions is rather due to the honest treatments of the incompressibility constraint and the non-linear terms. Instead, such treatments have led to relatively complicated procedures. Hence, there remains much room for improving the computational efficiency of the present procedure, by continuing further developments regarding, for example, a more efficient iterative solution technique, a solution procedure for large sets of simultaneous equations, and so on.

ACKNOWLEDGMENTS

This study has been supported by a Grant-in-Aid for Scientific Research from the Japanese Ministry of Education. Computations for this study were executed on the HITAC M-280H of the Computer Center of Tokyo Institute of Technology and the HITAC S-810 of the Computer Center of the University of Tokyo.

REFERENCES

1. O. C. Zienkiewicz, *The Finite Element Methods*, 3rd edn, McGraw-Hill, London, 1977.
2. D. H. Norrie and G. de Vries, 'A survey of the finite element applications in fluid mechanics', in R. H. Gallagher *et al.* (eds), *Finite Elements in Fluids*, Vol. 3, Wiley New York, 1978, Chap. 21, pp. 363–396.

3. P. Hood and C. Taylor, 'Navier–Stokes equations using mixed interpolation finite element in flow problems', in J. T. Oden *et al.* (eds), *Finite Element Methods in Flow Problems*, University of Alabama, Huntsville Press, 1974, pp. 121–143.
4. M. D. Olson and S.-Y. Tuann, 'Primitive variables versus stream function finite element solutions of the Navier–Stokes equations', in R. H. Gallagher *et al.* (eds), *Finite Elements in Fluids*, Vol. 3, Wiley, New York, 1978, Chap. 4, pp. 73–87.
5. P. S. Huyakorn, C. Taylor, R. L. Lee and P. M. Gresho, 'A comparison of various mixed-interpolation finite element in the velocity–pressure formulation of the Navier–Stokes equations', *Compt. and Fluids*, **6**, 25–35 (1978).
6. P. M. Gresho, R. L. Lee and C. D. Upson, 'FEM solution of the Navier–Stokes equations for vortex shedding behind a cylinder: experiments with the four-node element', *Adv. Water Res.*, **4**, 175–184 (1981).
7. R. L. Taylor and O. C. Zienkiewicz, 'Mixed finite element solution of fluid flow problems', in R. H. Gallagher *et al.* (eds) *Finite Elements in Fluids*, Vol. 4, Wiley, New York, 1982, Chap. 1, pp. 1–20.
8. L.-A. Ying and S. N. Atluri, 'A hybrid finite element method for Stokes flow, Parts 1 and 2', *Compt. Meth. Appl. Mech. Engng.*, **36**, 23–37 and 39–60 (1983).
9. C.-T. Yang and S. N. Atluri, 'An "assumed deviatoric stress-pressure-velocity" mixed finite element method for unsteady, convective, incompressible viscous flow: Parts 1 and 2', *Int. j. numer. methods fluids*, **3**, 377–398 (1983), and **4**, 43–69 (1984).
10. J. H. Argyris, J. St. Doltsinis, P. M. Pimenta and H. Wustenberg, 'Natural finite element techniques for viscous fluid motion', *Compt. Meth. Appl. Mech. Engng.*, **45**, 3–55 (1984).
11. T. J. R. Hughes, W. K. Liu and A. Brooks, 'Finite element analysis of incompressible viscous flows by the penalty function formulation', *J. Comp. Phys.*, **30**, 1–60 (1979).
12. M. Bercovier and M. Engelman, 'A finite element for the numerical solution of viscous incompressible flows', *J. Comp. Phys.*, **30**, 181–201 (1979).
13. J. C. Heinrich and R. S. Marshall, 'Viscous incompressible flow by a penalty function finite element method', *Comp. and Fluids*, **9**, 73–83 (1981).
14. J. N. Reddy, 'Penalty-finite-element analysis of 3-D Navier–Stokes equations', *Comp. Meth. Appl. Mech. Engng.*, **35**, 87–106 (1982).
15. J. T. Oden, 'RIP-methods for stokesean flows', in R. H. Gallagher *et al.* (eds), *Finite Elements in Fluids*, Vol. 4, Wiley, New York, 1982, Chap. 15, pp. 305–318.
16. J. Christies, D. F. Griffiths, A. R. Mitchell and O. C. Zienkiewicz, 'Finite element methods for second order differential equations with significant first derivations', *Int. j. numer. methods eng.*, **10**, 1389–1396 (1976).
17. J. C. Heinrich, P. S. Huyakorn and O. C. Zienkiewicz, 'An "upwind" finite element schemes for two-dimensional convective transport equation', *Int. j. numer. methods eng.*, **11**, 131–143 (1977).
18. J. Donea and S. Giuliani, 'A simple method to generate high-order accurate convection operators for explicit schemes based on linear finite elements', *Int. j. numer. methods fluids*, **1**, 63–79 (1981).
19. A. N. Brooks and T. J. R. Hughes, 'Streamline upwind/Petrov–Galerkin formulation for convection dominated flows with particular emphasis on the incompressible Navier–Stokes equations', *Com. Meth. Appl. Mech. Engng.*, **32**, 199–259 (1982).
20. P. M. Gresho, R. L. Lee and R. L. Sani, 'Advection-dominated flows, with emphasis on the consequences of mass lumping', in R. H. Gallagher *et al.* (eds), *Finite Elements in Fluids*, Vol. 3, Wiley, New York, 1978, Chap. 19, pp. 35–350.
21. P. M. Gresho, S. T. Chan, R. L. Lee and C. D. Upson, 'A modified finite element method for solving the time-dependent, incompressible Navier–Stokes equations. Part 1 and 2', *Int. j. numer. methods fluids*, **4**, 557–598 and 619–640 (1984).
22. J. Donea, S. Giuliani, H. Laval and L. Quartapelle, 'Finite element solution of the unsteady Navier–Stokes equation by a fractional step method', *Comp. Meth. Appl. Mech. Engng.*, **30**, 53–73 (1982).
23. M. Kawahara and H. Hirano, 'A finite element method for high Reynolds number viscous fluid flow using two step explicit scheme', *Int. j. numer. methods Fluids*, **3**, 137–163 (1983).
24. S. Taneda and H. Honji, 'Unsteady flow past a flat plate normal to the direction of motion', *J. Phys. Soc. Japan*, **30**, (1), 262–272 (1971).
25. A. Okajima, 'Strouhal numbers of rectangular cylinders', *J. Fluid Mech.*, **23**, 379–398 (1982).
26. A. Okajima and K. Sugitani, 'Flow around rectangular prism—numerical calculations and experiments, No. 2', *Bull. of Research Inst. for Appl. Mech.*, (50), 67–80 (1979) (in Japanese).
27. R. D. Blevins, *Flow-Induced Vibration*, Van Nostrand Reinhold Company, New York, 1977, Chap. 1.
28. M. Shimizu and Y. Tanida, 'On the fluid forces acting on rectangular sectional cylinders', *Trans. JSME (2)*, **44**, (384), 2699–2706 (1978) (in Japanese).
29. Y. Yoshida, N. Masuda and T. Fujiwara, 'A computational method for time integration of the heat conduction equations', in J. F. Abel *et al.* (eds), *Interdisciplinary Finite Element Analysis*, Cornell University, New York, 1981, 697–710.
30. Y. Yoshida, T. Fujiwara and T. Nomura, 'Direct time integration method for the transient heat conduction equation', *Proc. JSCE*, (313), 23–36 (1981) (in Japanese).
31. Y. Yoshida and T. Nomura, 'Application of the high accurate time integration to solution procedure of the Navier–Stokes equations', *Proc. JSCE*, (326), 29–40 (1982) (in Japanese).
32. Y. Yoshida, T. Nomura and R. Kanno, 'A solution procedure for the finite element equations of transient, incompressible, viscous flows', *Proc. JSCE*, (351), 59–68 (1984) (in Japanese).